*Thermal Science and Engineering* 2025, 8(1), 9883.
https://doi.org/10.24294/tse9883

Article

# Numerical analysis of closed loop pulsating heat pipe with varying condenser temperatures

**Sriram Chidambaranathan**

College of Engineering Guindy, Anna University, Chennai 600025, India; sriraamc86@gmail.com

**CITATION**

Chidambaranathan S. Numerical analysis of closed loop pulsating heat pipe with varying condenser temperatures. Thermal Science and Engineering. 2025; 8(1): 9883. https://doi.org/10.24294/tse9883

**ARTICLE INFO**

Received: 25 October 2024
Accepted: 19 December 2024
Available online: 2 January 2025



**Abstract:** A numerical investigation utilizing water as the working fluid was conducted on a 2D closed loop pulsating heat pipe (CLPHP) using the CFD software AnsysFluent19.0. This computational fluid dynamics (CFD) investigation explores three instances where there is a consistent input of heat flux in the evaporator region, but the temperatures in the condenser region differ across the cases. In each case, the condenser temperatures are set at 10 ℃, 20 ℃, and 30 ℃ respectively. The transient simulation is conducted with uniform time steps of 10 s. Generally, the heat rejection medium operated at a lower temperature performs better than at a higher temperature. In this CFD study the thermal resistances gets decreased with the decreasing value of condenser temperatures and the deviation of 35.31% of thermal resistance gets decreased with the condenser region operated at the temperature of 10 ℃.

**Keywords:** closed loop pulsating heat pipe; boiling and condensation; slug and plug flow; thermal resistance; Nusselt number

## 1. Introduction

With the rapid development of electronic components miniaturization, heat dissipation in the electronic components also proliferated. The performance of the electronic components is affected not only by the heat generated inside the components but also by temperature, which plays a major role. Therefore, proper thermal management is necessary to provide a stable operation in the electronic components. The heat pipe is mainly used to carry out the heat dissipation in the electronic components. The heat pipe is a passive heat exchanger device that transports heat with high thermal conductivity and low resistance. Out of the several types of heat pipes, a commonly used passive heat-exchanging device called a pulsating heat pipe is studied in this research work. The Closed-loop pulsating heat pipe is a two-phase heat transfer device that operates between the evaporator and condenser medium. According to Akachi [1], a pulsating heat pipe is a long metallic capillary tube with an internal dimension small enough to enable compressed two-phase working fluid, which is sealed inside the metallic capillary tube. Wu et al. [2] investigated experimentally and numerically refrigerant flow boiling in horizontal serpentine tubes, and they concluded that the stratification flow exists in the horizontal tube and the buoyancy force is dominant against gravity. Rudresha et al. [3] study deals with the experimental as well as numerical investigation of the thermal performance of CLPHP charged with DI water and Nanofluids such as $SiO_2$/DI Water and $Al_2O_3$/DI Water, and he found that the heat transfer coefficient gets increased with Nanofluids than DI Water. Erfan et al. [4] made a comparison of a four-turn aluminum flat plate PHP and an additional branch on the evaporator section on the same. The authors investigated different filling ratios and heat inputs,

which showed that the thermal resistance decreased by up to 11%–20% by using an additional branch on the evaporator section on the four-turn PHP. Pramod et al. [5] did experimental work on two turn copper closed loop pulsating heat pipe with a single component fluid such as water, ethanol, methanol, and acetone and also with binary mixtures such as water-ethanol, water-methanol, and water-acetone. The authors validated the experimental results numerically, and his results show that thermal performance was increased with the use of working fluid as a binary mixture of water-acetone. Anwar et al. [6] study deals with an investigation of seven-turn CLPHP with water as a working fluid in which the evaporator section is heated employing hot air with different velocities such as 0.5, 1, and 1.5 m/s, and proposed that the thermal resistance was found low with high heat input. He also compared the experimental investigation with a CFD study of maximum heat input of 107.75 W and with the minimum heat input of 13.75 W corresponding to the air inlet temperature. Karthikeyan et al. [7] investigated eight-turn copper pulsating heat pipes with water as a working fluid, and the wall temperatures were measured employing high-resolution infrared thermography, in which the authors studied the flow behavior inside the CLPHP also concluded that the thermal resistance was found lower with the heat input increased from 30 W to 500 W. Duy-Tan et al. [8] investigated experimentally and numerically with eight-turn PHP using working fluid as R123, and they found that the CFD analysis work matches the experimental work with the use of the k-ϵ turbulence model. Przemyslaw et al. [9] validated the numerical model with the experimental data on a three three-turn PHP with ethanol as a working fluid and stated that the relative error was obtained at a 10% level. Nick et al. [10] investigated the effect of condenser temperatures in a PHP, and they concluded that lower thermal resistance was obtained by increasing condenser temperatures. Jiaqiang et al. [11] did a numerical investigation on single-turn and two-turn CLPHP by considering the VOF model. He found that the double-turn CLPHP has higher heat transfer capability than the single-turn CLPHP. Jiansheng et al. [12] analyzed numerically a CLPHP with a partial horizontal structure (Evaporator and Condenser Sections are horizontal) by varying filling ratios and heat flux, and in which the author's results reveal that when the height difference between the evaporator and condenser section is more the thermal performance gets increased. Qingfeng et al. [13] numerical work deals with the anti-dry out in the evaporator section of the CLPHP with the use of micro-encapsulated phase change material, and his study proves that the start-up time, circulation of flow, and heat transfer performance were improved significantly with the use of phase change material compared with water. Kalpak et al. [14] conducted a 2D simulation of CLPHP with liquid Nitrogen as a working fluid. It was tested with ground level, low gravity, and milli-gravity conditions with different filling ratios. The authors concluded that more stable flow patterns and heat transfer performance were observed in low-gravity conditions when compared with ground-level conditions. Fubo et al. [15] investigated numerically a single-turn CLPHP with two different evaporator geometries, such as a round end and a right-angled end with different heat inputs and in which he proposed a result of later geometry shows rarely the stop-over phenomenon and an increased heat transfer performance. Zirong et al. [16] work deals with the miniature oscillating pulsating heat pipes in which the authors used the

VOF approach with different models in the numerical work; in addition to that, the authors worked on changing the heating source length, internal diameter, and heat input power and the authors concluded that the internal diameter of the OPHP plays a vital role. Hyung et al. [17] made a one-dimensional model assuming liquid slug/vapor plug flow by considering the phase interactions between the solid wall and the liquid film. They also validated the experimental data which is available in the literature. Finally, the authors concluded that by choosing the high merit number (criterion for selecting working fluids), the thermal performance of the CLPHP is maximized. Zufar et al. [18] made 2D simulations on CLPHP with water-based Nano fluids such as Diamond, Silver, and Silica Oxide. The authors studied numerically with constant heat flux and filling ratio and came up with the outcome of diamond-based nanofluids performing better with lower thermal resistance. Jongwook et al. [19] investigated a 2D CLPHP numerically with ethanol as the working fluid in a multi-turn geometry with symmetric and asymmetric modes. The authors predicted that the starting time of the CLPHP with an asymmetric shape is earlier than with a symmetric shape. Also, he found that in the case of zero gravity, the fluid gets dried out in the case of 5 and 10 turns, whereas the fluid remains in the evaporator section in the case of 15 and 20 turns, respectively. Jiansheng et al. [20] research work deals with the simulation of 2D single loop CLPHP with varying.

Heat input from 10 W to 40 W and varying filling ratios from 30% to 60%, respectively, and the authors found that the thermal resistance decreased with the high heat input and also with the same filling ratio and input power also the authors varied the condenser length of the CLPHP in which he observed that the start-up time gets accelerated. Ayad et al. [21] analyzed wickless heat pipe using a commercial CFD package, and the flow behavior, heat transfer features, and boiling regimes were studied using their inbuilt user-defined functions. Also, the wickless heat pipe was investigated with different filling ratios, inclination angles, and heat added. Jiansheng et al. [22] performed a 3D simulation in comparison with deionized water and a surfactant called hexadecyl trimethyl ammonium chloride by changing the initial pressure and heat input. The authors suggested that by using surfactant as a working fluid under high initial pressure, the performance of CLPHP was not good. With low initial pressure, its performance also increases, and the heat transfer performance of CLPHP increases with high heat inputs; thereby, the use of surfactants prevents the drying out of the evaporator section. The above-discussed literature shows that the CFD analysis was carried out with fixed evaporator heat input and constant condenser temperatures. This research work entails a numerical investigation focusing on fixed evaporator heat flux boundary conditions while examining the relatively underexplored aspect of varying condenser temperatures. A 2D computational fluid dynamics (CFD) analysis is conducted using water as the working fluid, with the condenser temperatures manipulated to be below ambient temperature.

## 2. Research methodology

The current research methodology encompasses several key steps, including geometry creation, meshing, and solver setup. This involves selecting appropriate

models, patching, probe setup, and determining the precise time step size. This present numerical work focuses on the literature [10] and it can be validated to some extent The following section provides a brief overview of the aforementioned research

## 2.1. Geometry of CLPHP

A thorough literature survey has been carried out, and based on the literature, [23] the following geometry as shown in the **Figure 1** has been selected for the numerical work. The geometry is set as two turns with equal dimensions of the evaporator, adiabatic, and condenser sections, and the internal diameter is 2 mm throughout the pipe.

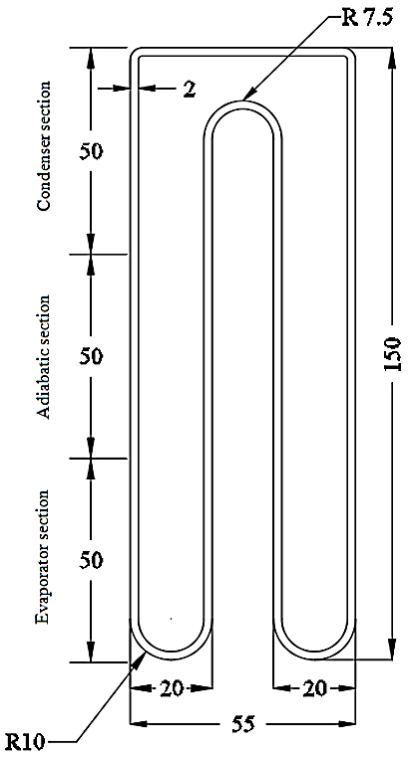


**Figure 1.** Geometry of CLPHP.

Note: All dimensions in 'mm'.

## 2.2. Meshing

Meshing is done by using Hypermesh Software and Quadrilateral elements are used for meshing. **Figures 2** and **3** describes the meshing of the CLPHP. The details of the mesh are described below in **Table 1**.

**Table 1.** 2D mesh description.

| Total Nodes | Total elements | Size of the Elements | Type of mesh |
|---|---|---|---|
| 23,661 nodes | 21,032 elements | 0.25 mm | Quadrilateral mesh |

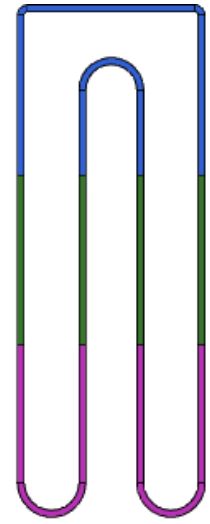

**Figure 2.** 2D meshing of CLPHP.

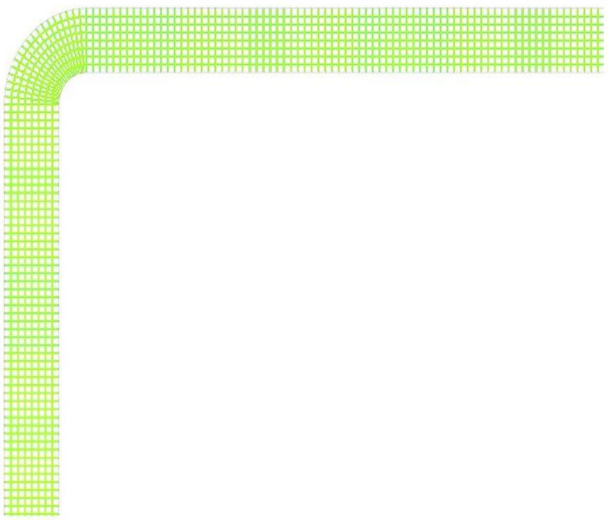

**Figure 3.** Cut section of 2D mesh of CLPHP.

## 2.3. Multiphase flow analysis (VOF)

The problem is based on multiphase flow; the VOF model is chosen, and 3 phases have been selected in the GUI. The 3 phases include water liquid, water vapor, and air. We know that all CFD simulations have a set of governing equations: continuity or mass, momentum, and energy equations. Here, the VOF model is based on multiphase flow. It has a separate equation that includes phase fraction, which has to be solved for both liquid and vapor phases. The VOF governing equations are discussed below.

## 2.4. Governing equations

The flow inside the CLPHP consists of liquid slugs and vapor plugs, which are immiscible fluids. To track the immiscible fluids (liquid-gas), the VOF approach is generally used, and the phase fraction ($\alpha$) is used to calculate the distinct phases. The condition for the phase fraction ($\alpha$) was revisited and rephrased for accuracy and clarity. Specifically, the definition now explicitly states that $\alpha$ represents the local

volumetric fraction of the liquid or vapor phase and satisfies the condition $0 \leq \alpha \leq 1$. There exists a condition for phase fraction ($\alpha$), which is given by:

When $\alpha_q = 0$, the cell is empty (No fluids present), $\alpha_q = 1$, the cell is filled with fluid (Full fluid is present), and $0 < \alpha_q < 1$, the cell has a mixture of two or three fluids.

## 2.5. Mass equation

In CLPHP the evaporation and condensation phenomenon takes place, the liquid-vapor mass transfer is governed by the vapor transport Equation (1) and it is given by:

$$\frac{\partial(\alpha_v \rho_v)}{\partial t} + \nabla.(\alpha_v \rho_v v_v) = \dot{m}_{lv} - \dot{m}_{vl} \tag{1}$$

In the case of evaporation, $T_l > T_{sat}$

$$\dot{m}_{lv} = r_{lv}.\alpha_l \rho_l \frac{(T_l - T_{sat})}{T_{sat}} \tag{2}$$

In the case of condensation, $T_v < T_{sat}$

$$\dot{m}_{vl} = r_{vl}.\alpha_v \rho_v \frac{(T_{sat} - T_v)}{T_{sat}} \tag{3}$$

## 2.6. Momentum equation

A single set of momentum Equation (4) is solved throughout the domain, which is given by:

$$\frac{\partial(\rho\vec{v})}{\partial t} + \nabla.(\rho\vec{v}\vec{v}) = -\nabla P + \nabla.[\mu(\nabla\vec{v} + \nabla\vec{v}^T)] + \rho\vec{g} + \vec{F}_{vol} \tag{4}$$

The surface tension arises because of the cohesive force of the molecules, and it creates a surface force that is added to the source term in the momentum equation. This force in the surface is called volume force, and it is given by:

$$F_{vol} = \sigma_{lv} \frac{\alpha_l \rho_l k_v \nabla\alpha_v + \alpha_v \rho_v k_l \nabla\alpha_l}{\frac{1}{2}(\rho_l + \rho_v)} \tag{5}$$

where the curvature is expressed as

$$k_l = \frac{\Delta\alpha_l}{\nabla\alpha_v} \text{ and } k_v = \frac{\Delta\alpha_v}{\nabla\alpha_l}$$

## 2.7. Energy equation

The energy shared by the phases Equation (6) is given by the equation:

$$\frac{\partial(\rho E)}{\partial t} + \nabla.(\vec{v}(\rho E + P) = \nabla.(K.\nabla T) + S_h \tag{6}$$

where $S_h$ is the source term caused by the phase change obtained by multiplying the mass transfer rate by the latent heat.

The expressions for energy shared by the two phases are given by:

$$E = \frac{\alpha_l \rho_l E_l + \alpha_v \rho_v E_v}{\alpha_l \rho_l + \alpha_v \rho_v} \tag{7}$$

where the specific heat of the phases is given by:

$$E_l = C_{v,l}(T - T_{sat}) \tag{8}$$

$$E_v = C_{v,v}(T - T_{sat}) \tag{9}$$

The properties like $\rho$, $K$, and $\mu$ shared by the phases are given by:

$$\rho = \alpha_l \rho_l + \alpha_v \rho_v \tag{10}$$

$$K = \alpha_l K_l + \alpha_v K_v \tag{11}$$

$$\mu = \alpha_l \mu_l + \alpha_v \mu_v \tag{12}$$

## 2.8. Setting the probe

The temperature in the evaporator, adiabatic, and condenser sections has to be monitored till the given time steps so that the analytical calculations can be made easily. As the geometry is 2D and the CLPHP is made in two loops, the temperature in each loop of the evaporator section, adiabatic section, and condenser section must be monitored to take the average values. In total, six probes have to be set in the 2D geometry, of which two probes monitor the temperature in the evaporator section, two probes monitor the temperature in the adiabatic section, and two probes monitor the temperature in the condenser section, respectively. From the 2D geometry, the probes are set in the monitor tab in the GUI of fluent, in which points are created in the locations of the evaporator, adiabatic, and condenser sections. In total, six points are designed and created by measuring the *X* and *Y* coordinates of the geometry. These created points are then renamed so the data extracted can be easily identified. The probes in the evaporator section are renamed as Te1 and Te2, the probes in the adiabatic section are renamed as Ta1 and Ta2, and the probes in the condenser section are renamed as Tc1 and Tc2, respectively. The suffix indicates the location in the first and second loops of the CLPHP. After renaming the probes under the monitor option in the GUI report, a plot is selected for the selected probes so that the temperature in each section is extracted for the given number of time steps while running the simulation and saved in a separate text file. These temperature data in the evaporator, adiabatic, and condenser sections are then used analytically to calculate thermal resistance and heat transfer coefficient. The below **Figure 4** shows the probes which has been set in the CLPHP.

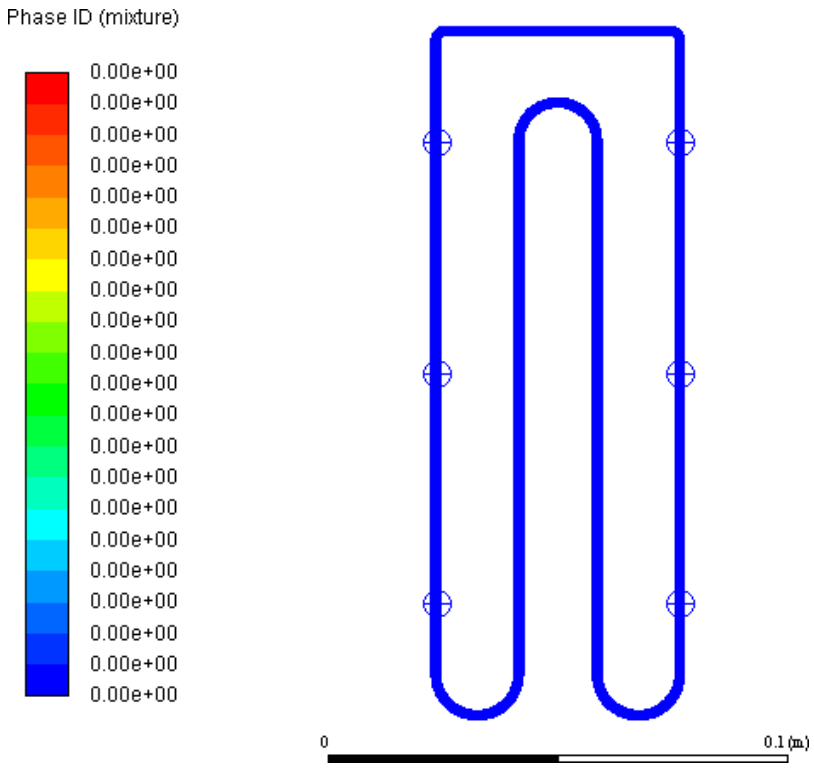


**Figure 4.** Probes representation in the CLPHP.

## 2.9. Initializing and patching

The solution is initialized first in the solution initialization option present in the GUI, and the standard initialization iteration method is selected in this simulation. The temperature in the fluid domain is initialized as 303 K, as the simulation has been done for three different condenser wall temperatures of 10 ℃, 20 ℃, and 30 ℃, and the liquid volume fraction and air volume fraction is set as '0' because the next step is to fill the liquid water and air inside the CLPHP. Patching is filling the fluid inside the CLPHP with a suitable proportion. Liquid water and air are patched inside the CLPHP, considering liquid water is patched to 50% of the total volume, and the remaining 50% constitutes the air volume. We can notice from the geometry that the evaporator is at the bottom, and heat flux is applied to it, so the water has to be patched from the bottom of the geometry.

The geometry is created with a total height of 150 mm; as we know, the evaporator, adiabatic, and condenser sections comprise 50 mm each, half of the total height, i.e., 75 mm from the bottom has to be patched with the liquid water and the remaining volume is patched as air. To create a patch for the liquid water in the CLPHP, an option called mark is there in the region where the coordinates are given for patching the liquid water, and then the volume fraction is set to '1'. The same procedure is done for patching the air in the remaining portion of the CLPHP. After patching the liquid water and air in the CLPHP, the new data is created, which indicates the initial time step, i.e., at 0 s, from which the simulation was started. The **Figure 5** below shows the liquid water and air volume fractions created in the CLPHP.

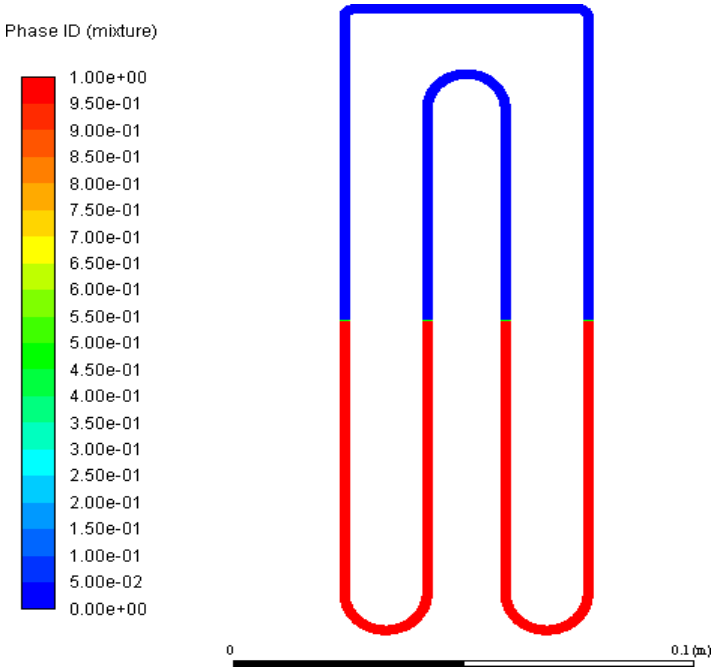


**Figure 5.** Liquid patch representation on CLPHP.

## 2.10. Case setting in fluent

In the general tab, the following setting is done. They are as follows:

a) Type of Solver—Pressure based solver is used in this current work and as the working fluid used is incompressible water, the analysis has to be carried out on the same.

b) Time—Transient is used. In the multiphase analysis, the phase fraction has to be calculated in each time step, and generally, PHP works in an unsteady state. Therefore, the transient state is selected.

c) Gravity—The orientation of the CLPHP is vertical (i.e. 90°). The acceleration due to gravity is taken in the negative Y axis, given as −9.81 m/s$^2$.

## 2.11. Viscous model

In order to find whether the flow is laminar or turbulent, it is necessary to calculate the Reynolds number. The Reynolds number (13) is given by,

$$\mathrm{Re} = \frac{\rho \times v \times d}{\mu} \tag{13}$$

where the density ($\rho$) and kinematic viscosity ($\mu$) are taken from the saturation pressure and temperature, as we know that the PHP is operated under vacuum, the operating pressure is taken as 4000 pascals, [24] which is studied from the literature. The saturation pressure is found to be 0.04 bar, from which the saturation temperature must be calculated. The saturation temperature is calculated from the Antoine equation, which is given below.

In general, the Antoine Equation (14) is given as:

$$\log_{10}(P) = A - \frac{B}{T + C} \tag{14}$$

where *A*, *B*, and *C* are constants.

$$\log_{10}(0.04) = 5.31384 - \frac{1690.864}{T - 51.804} \tag{15}$$

$$-1.39794 + \frac{1690.864}{T - 51.804} = 5.31384 \tag{16}$$

$$\frac{1690.864}{T - 51.804} = 5.31384 + 1.39794 \tag{17}$$

$$6.71178T - 347.69705 = 1690.864 \tag{18}$$

$$6.71178T = 2038.56105 \tag{19}$$

$$T = 303.72 \text{ K} \tag{20}$$

$$T = 30 \text{ ℃} \tag{21}$$

Thus, the saturation temperature is 30 ℃, corresponding to the saturation pressure of 4000 Pa or 0.04 bar.

With the above data of saturation temperature and pressure, the properties of water liquid, water vapor, and air can be taken from the available resources. The following **Table 2** shows the properties of water liquid, water vapor, and air at a saturation temperature of 30 ℃ and saturation pressure of 0.04 bar.

**Table 2.** Properties of water at a saturation temperature of 30 ℃.

| **Fluid** | **Density ($\rho$) (kg/m$^3$)** | **Dynamic Viscosity ($\mu$) (kg/ms)** | **Specific Heat ($C_p$) (kj/kgK)** | **Thermal Conductivity (K) (W/mK)** | **Surface Tension ($\sigma$) (N/m)** |
|---|---|---|---|---|---|
| Water (liquid) | 995.91 | 0.00081 | 4.180 | 0.613 | 0.07 |
| Water (Vapor) | 0.0287 | 0.000009 | 1.916 | 0.018 | |
| Air | 0.0461 | 0.000018 | 1004.83 | 0.027 | |

Now, the Reynolds number calculated based on Equation (13) is 2213.13.

We know that when the Re < 2300, the flow is said to be laminar. Therefore, a laminar viscous model is chosen to simulate the fluid flow in the CLPHP.

## 2.12. Phase definition and phase interactions

This work has three phases: liquid, vapor, and air. In the VOF approach, all three phases have to be defined. The phase descriptions are as follows.

1) Water vapor—Primary phase;
2) Water liquid—Secondary phase;
3) Air—Secondary phase.

In addition to the phase definitions, the phase interactions must also be defined. Phase interactions are nothing but mass transfer and surface tension. Mass transfer occurs in the CLPHP due to its evaporation and condensation, and as the pipe diameter is so slight, surface tension plays an important role. It also has to be adequately defined. At saturation temperature, the liquid turns to vapor, and the vapor turns liquid. So, the evaporation–condensation mechanism is defined as the

mass interaction from the vapor to the liquid phase. The Continuum surface force (CSF) model modeled the surface tension force, and the constant value of 0.07 N/m is given as input to the surface tension coefficient.

### 2.13. Boundary conditions

The CLPHP geometry is divided into three zones: evaporator in the bottom, adiabatic zone in the middle, and condenser in the top. All three sections are equally divided with a height of 50 mm, each having an inner diameter of 2 mm. As we discussed before, the liquid water is patched to 50% of the total volume of the CLPHP, and the remaining portion is filled with air. Generally, the boundary conditions are given at the walls of the sections,

and here, they are given at the evaporator, adiabatic, and condenser sections. The heat flux given at the walls of the evaporator gives rise to the temperature, and the heat gets rejected at the condenser, producing a pulsation effect. Zero heat flux is given at the adiabatic zone so that no heat transfer occurs in this zone. In this work, the evaporator and adiabatic zone wall conditions are fixed, and the condenser wall temperature is changed in all three cases to investigate the effect of the thermal performance of CLPHP. The boundary conditions used in this analysis in all three cases are discussed below:

a) Evaporator—constant heat flux of 10,000 w/m$^2$ [25] having a wall thickness of 0.005 m (Neumann).
b) Adiabatic—constant heat flux of 0 w/m$^2$ having a wall thickness of 0.005 m (Neumann).
c) Condenser—Temperature of 10 ℃, 20 ℃, and 30 ℃ (Dirichlet).

## 3. Numerical analysis results

The probes fixed in the each section of the CLPHP reads the temperature values in each time step size and the evaporator and condenser temperature values are taken into consideration for analyzing the results of all 3 cases.

### 3.1. Temperature vs. time plot

The following plots discuss the temperature monitored from the evaporator and condenser section for time steps of 10 s. In two-turn CLPHP, two probes are fixed in the evaporator, adiabatic, and condenser sections in each loop, respectively. Therefore, an average of evaporator temperature (Te) and condenser temperature (Tc) are calculated, and the graph is plotted against time.

**Figure 6** represents the plot between the average evaporator and condenser temperature against time for the condenser temperature fixed at 10 ℃. Due to high heat flux, the evaporator temperature is increased to a maximum value. The non-linear trend in the evaporator temperature is due to the probes fixed in the surface of the 2D CLPHP geometry measures the liquid slug temperature as well as the vapor plug temperature. We know that as the vapor plug density is lower compared to the liquid slug, the temperature in the vapor plug is higher than the temperature in the liquid slug. During the simulation for a total timestep, when the vapor plug comes into contact with the probes fixed in any one turn of the evaporator section the

temperature is drastically increased compared to the liquid slug temperature. Therefore, a sharp rise in the average evaporator temperature was observed during the analytical calculations. As the wall of the condenser temperature was fixed as 283 K it shows a linear variation throughout the timesteps found to be decreased slighter.

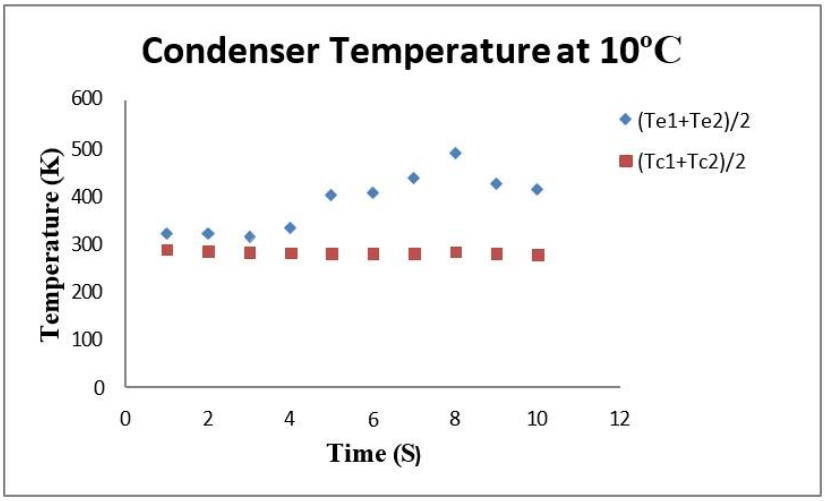


**Figure 6.** Temperature versus time for the condenser temperature at 10 ℃.

**Figure 7** shows the average temperature variation of evaporator and condenser section over time when the condenser wall temperatures are fixed at 20 ℃. Similar observation was found in the average condenser temperature whereas the average evaporator temperature was found to be increasing non-linearly.

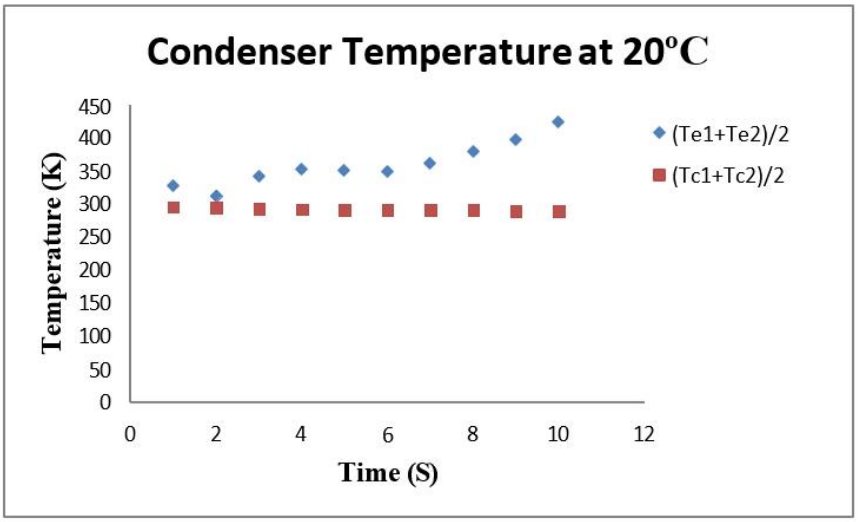


**Figure 7.** Temperature versus time for the condenser temperature at 20 ℃.

**Figure 8** shows the temperature against time of average evaporator and condenser sections, when the condenser walls are prescribed at ambient temperature i.e 30 ℃. Similar observations were found as in the above 2 cases, the only difference observed is that the average evaporator temperature is found increased.

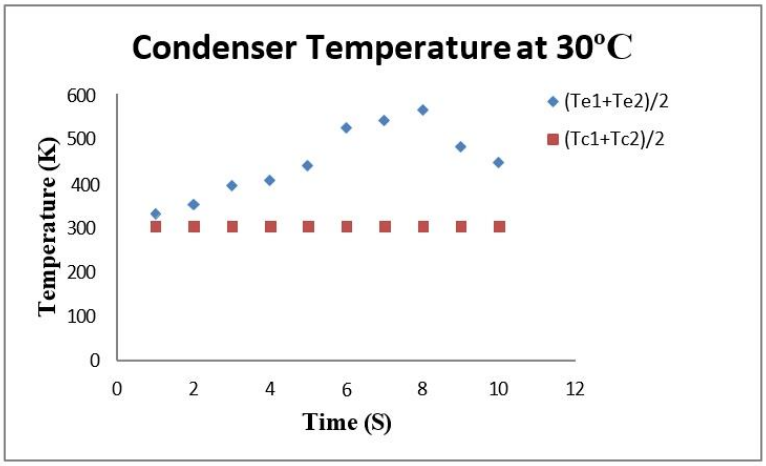


**Figure 8.** Temperature versus time for the condenser temperature at 30 ℃.

We clearly observe that when the condenser walls are maintained at 10 ℃ it absorbs more heat compared to other 2 cases and the temperature difference of evaporator and condenser sections are found low compared with condenser walls are fixed at 20 ℃ and 30 ℃. As we know that with the input heat flux, when the temperature difference of evaporator and condenser sections are low then the thermal resistance gets decreased and the heat transfer coefficient also found to be increased. From this numerical analysis it is clearly observed that the thermal performance of the 2D CLPHP is increased when the condenser temperature is fixed at 10 ℃. Due to the limited computational resources the simulations were performed only for the time steps of 10 s. If the simulations were carried out for more number of time steps then the temperature difference of evaporator and condenser section was found too low and the thermal performances can be compared well for all the 3 cases.

## 3.2. Contours of CLPHP

The distinct phases like liquid and vapor are visualized after simulating for the given time steps and are shown below.

The above **Figure 9** represents the contour of the phase mixture i.e the liquid and vapor phases can be observed clearly. This contour shows the liquid slug and vapor plug oscillation takes place inside the CLPHP.

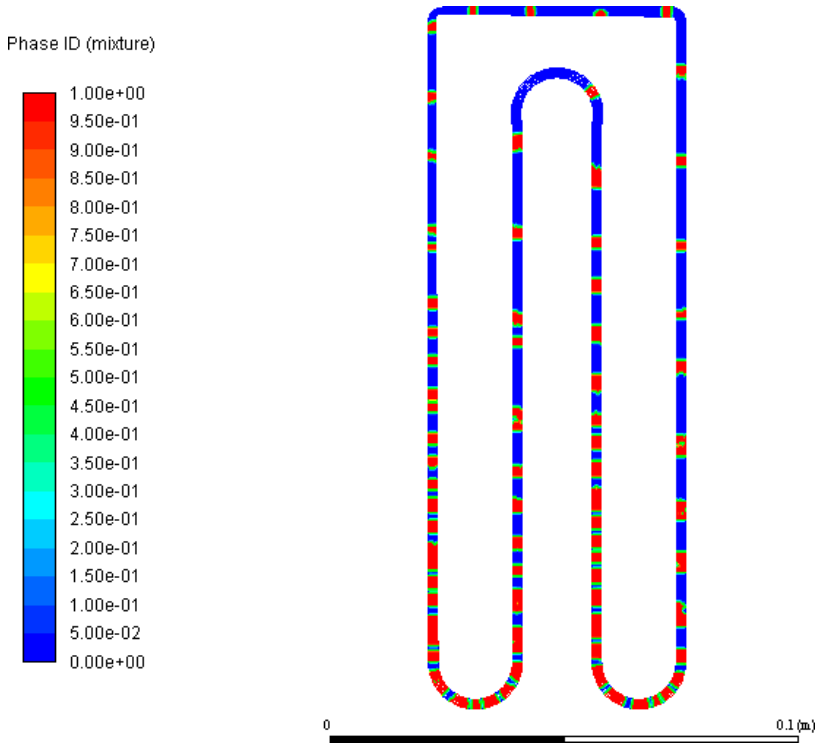


**Figure 9.** Contour for the phase mixture in the CLPHP.

The above **Figure 10** shows the volume fraction of the vapor phase exist inside the CLPHP for certain time steps. It is noted that the liquid and vapor phase can be observed throughout the CLPHP.

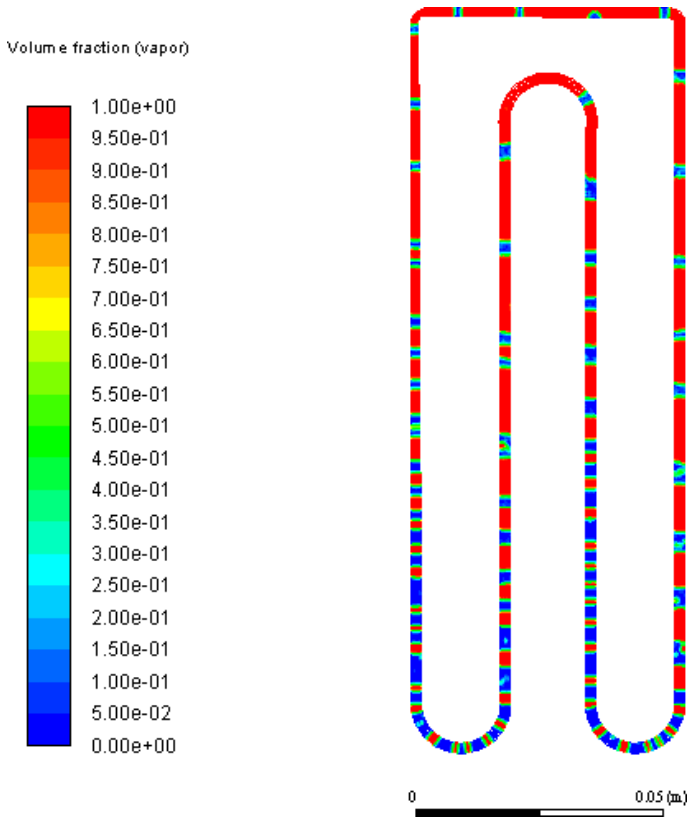


**Figure 10.** Contour for the volume fraction in the CLPHP.

### 3.3. Nusselt number calculation

In general, Nusselt number (Nu) is the ratio of convective heat transfer to the conductive heat transfer in a fluid. It is a dimensionless number and it indicates the heat transfer takes place in a fluid medium is by conduction or convection.

The Nusselt number is given by:

$$\mathrm{Nu} = \frac{hL}{K}$$

The Nusselt number range represents the heat transfer characteristics in a fluid flow and it is given as:

If Nu = 0, Pure conductive heat transfer;

If 0 < Nu < 10, Slug flow or laminar flow;

If 100 < Nu < 1000, High convective heat transfer or Turbulent flow.

In this present numerical work the Nusselt number was calculated for all the 3 cases from the temperature datas measured with the help of probes. The Nusselt number was calculated analytically and it is found to be within 1 in all the 3 cases which is shown above in **Table 3**. The highest Nusselt number was obtained from the case of condenser temperature fixed at 10 ℃. The Nusselt number range in the present simulation indicates the slug flow or laminar flow which can be observed from the available contours.

**Table 3.** Nusselt number values for different condenser temperatures.

| **Temperature (℃)** | **10** | **20** | **30** |
|---|---|---|---|
| Nusselt Number | 0.9311 | 0.8807 | 0.8576 |

## 4. Conclusion

In the case of CFD analysis water is used as a working fluid and the analysis work was carried out with 2D CLPHP geometry. As discussed about the geometry creation, meshing and the solver setting in the above section brief conclusions are made which are discussed below. They are as follows.

- With constant heat flux at the evaporator and by varying the temperatures of the condenser sections of about 10 ℃, 20 ℃ and 30 ℃ the CLPHP shows a better performance with the condenser temperature of 10 ℃.
- In this analysis for all the 3 cases a constant time of up to 10 s has been calculated for the transient analysis and the results plotted above was only for up to 10 s.
- The contours of phase fraction shows the liquid slug and vapor plug inside the CLPHP and with the further time steps better results can be obtained.
- The Nusselt number calculation from all the 3 cases shows the slug flow or laminar flow.

**Conflict of interest:** The author declares no conflict of interest.

## Nomenclature

| | |
|---|---|
| PHP | Pulsating Heat Pipe |
| DI | De-ionized Water |
| $C_v$ | specific heat, J/kg K |
| P | pressure, bar |
| E | internal energy, KJ/kg |
| g | acceleration due to gravity, m/s$^2$ |
| T | temperature, K |
| v | velocity, m/s |
| D | diameter, mm |
| h | heat transfer coefficient, w/m$^2$K |
| L | characteristic length, m |

## Greek symbols

| | |
|---|---|
| $\alpha$ | volume fraction |
| $\mu$ | dynamic viscosity |
| $\rho$ | density |
| $\sigma$ | surface tension |

## Subscripts

| | |
|---|---|
| a | adiabatic section |
| c | condenser section |
| e | evaporator section |
| l | liquid |
| SAT | saturation |
| V | vapor |

## References

1. Akachi H. Structure of Heat Pipe. U.S. Patent Application No. 5,219,020. 1990.
2. Wu HL, Peng, XF, Ye P, Eric Gong, Y, Simulation of Refrigerant Flow Boiling in Serpentine Tubes. International Journal of Heat and Mass Transfer. 2007; 50(5–6): 1186–1195. doi: 10.1016/j.ijheatmasstransfer.2006.10.013
3. Kumar V, Rudresha S. CFD Analysis and Experimental Investigation on Thermal Performance of Closed Loop Pulsating Heat Pipe Using Different Nanofluids. International Journal of Advanced Research. 2014; 2(8): 753–760.
4. Sedighi E, Amarloo A, Shafii B. Numerical and Experimental Investigation of Flat-Plate Pulsating Heat Pipes with Extra Branches in the Evaporator Section. International Journal of Heat and Mass Transfer. 2018; 126: 431–441. doi: 10.1016/j.ijheatmasstransfer.2018.05.047
5. Pachghare PR, Mahalle AM. Thermo-Hydrodynamics of Closed Loop Pulsating Heat Pipe: An Experimental Study. Journal of Mechanical Science and Technology. 2014; 28(8): 3387–3394. doi: 10.1007/s12206-014-0751-9
6. Barrak AS, Saleh AAM, Naji ZH. Experimental and Numerical Simulation for Thermal Investigation of Oscillating Heat Pipe Using VOF Model. Engineering and Technology Journal. 2020; 38: 88–104.
7. Karthikeyan VK, Khandekar S, Pillai BC, et al. Infrared Thermography of a Pulsating Heat Pipe: Flow Regimes and Multiple Steady States. Applied Thermal Engineering. 2014; 62(2): 470–480. doi: 10.1016/j.applthermaleng.2013.09.041
8. Vo DT, Kim HT, Ko J, et al. An Experiment and Three-Dimensional Numerical Simulation of Pulsating Heat Pipes. International Journal of Heat and Mass Transfer. 2020; 150: 119317. doi: 10.1016/j.ijheatmasstransfer.2020.119317

9. Błasiak P, Opalski M, Parmar P, et al. The Thermal—flow Processes and Flow Pattern in a Pulsating Heat Pipe—numerical Modelling and Experimental Validation. Energies. 2021; 14(18). doi: 10.3390/en14185952
10. Hansen N, Versteeg J, Michna GJ. Effect of Condenser Temperature on Pulsating Heat Pipe Performance. In: Proceedings of the ASME 2013 Heat Transfer Summer Conf; 14–19 July 2013; Minneapolis, MN, USA. pp. 1–6.
11. Jiaqiang E, Zhu R, Zuo H, et al. Simulation and Analysis on Heat Transfer Performance of Oscillating Heat Pipe with Single and Double Passageway. Advanced Materials Research. 2012; 516–517: 433–37. doi: 10.4028/www.scientific.net/AMR.516-517.433
12. Wang J, Bai X. The Features of CLPHP with Partial Horizontal Structure. Applied Thermal Engineering. 2018; 133: 682–89. doi: 10.1016/j.applthermaleng.2018.01.058
13. Li Q, Wang Y, Lian C, et al. Effect of Micro Encapsulated Phase Change Material on the Anti-Dry-out Ability of Pulsating Heat Pipes. Applied Thermal Engineering. 2019; 159: 113–854. doi: 10.1016/j.applthermaleng
14. Kalpak RS, Naik HB, Mehta HB. CFD Analysis of Cryogenic Pulsating Heat Pipe with Near Critical Diameter under Varying Gravity Conditions. Theoretical Foundations of Chemical Engineering. 2020; 54(1): 64–76. doi: 10.1134/S0040579520010212
15. Xie F, Li X, Qian P, et al. Effects of Geometry and Multisource Heat Input on Flow and Heat Transfer in Single Closed-Loop Pulsating Heat Pipe. Applied Thermal Engineering. 2019; 168: 114856. doi: 10.1016/j.applthermaleng.2019.114856
16. Lin Z, Wang S, Shirakashi R, et al. Simulation of a Miniature Oscillating Heat Pipe in Bottom Heating Mode Using CFD with Unsteady Modeling. International Journal of Heat and Mass Transfer. 2013; 57(2): 642–656. doi: 10.1016/j.ijheatmasstransfer.2012.09.007,
17. Noh HY, Kim SJ. Numerical Simulation of Pulsating Heat Pipes: Parametric Investigation and Thermal Optimization. Energy Conversion and Management. 2020; 203: 112237. doi: 10.1016/j.enconman.2019.112237
18. Zufar M, Gunnasegaran P, Ching Ng K. Numerical Study on the Effects of using Nanofluids in Pulsating Heat Pipe. International Journal of Engineering & Technology. 2018; 7(4): 6.
19. Choi J, Zhang Y. Numerical Simulation of Oscillatory Flow and Heat Transfer in Pulsating Heat Pipes with Multi-Turns Using OpenFOAM. Numerical Heat Transfer; PartA: Applications. 2020; 77(8): 761–781. doi: 10.1080/10407782.2020.1717202
20. Wang J, Ma H, Zhu Q. Effects of the Evaporator and Condenser Length on the Performance of Pulsating Heat Pipes. Applied Thermal Engineering. 2015; 91: 1018–1025. doi: 10.1016/j.applthermaleng.2015.08.106
21. Al Jubori AM, Jawad QA. Computational Evaluation of Thermal Behavior of a Wickless Heat Pipe under Various Conditions. Case Studies in Thermal Engineering. 2020; 22: 100767. doi: 10.1016/j.csite.2020.100767
22. Wang J, Xie J, Liu X. Investigation on the Performance of Closed-Loop Pulsating Heat Pipe with Surfactant. Applied Thermal Engineering. 2019; 160: 113998. doi: 10.1016/j.applthermaleng.2019.113998
23. Chidambaranathan S, Rangaswamy SM. Experimental Investigation of Higher Alcohols as Self-Rewetting Fluids in Closed Loop Pulsating Heat Pipes. Thermal Science. 2021; 25: 781–790. doi: 10.2298/TSCI200509347C
24. Sedighi E, Amarloo A, Shafii B. Numerical and experimental investigation of flat-plate pulsating heat pipes with extra branches in the evaporator section. International Journal of Heat and Mass Transfer. 2018; 126: 431–441. doi: 10.1016/j.ijheatmasstransfer.2018.05.047
25. Costa Bitencourt, Umberto. (2016). CFD simulation of a Pulsating Heat Pipe using ANSYS FLUENT. Available online: https://www.researchgate.net/publication/305608515 (accessed on 15 November 2024).